Bioorganic Chemistry 36 (2008) 278–287

Contents lists available at ScienceDirect

Bioorganic Chemistry

journal homepage: www.elsevier.com/locate/bioorg

DNA-binding and photocleavage properties of cationic porphyrin–anthraquinone hybrids with different lengths of links

Ping Zhao [a], Lian-Cai Xu [b], Jin-Wang Huang [a,c,*], Bo Fu [a], Han-Cheng Yu [a], Wei-Hong Zhang [d], Jian Chen [d], Jun-Hua Yao [d], Liang-Nian Ji [a,c]

[a] MOE Laboratory of Bioinorganic and Synthetic Chemistry, School of Chemistry and Chemical Engineering, Sun Yat-Sen University, No. 135, Xingangxi Road, Guangzhou 510275, PR China
[b] Center for Computational Quantum Chemistry, South China Normal University, Guangzhou 510631, PR China
[c] State Key Laboratory of Optoelectronic Material and Technologies, Sun Yat-Sen University, Guangzhou 510275, PR China
[d] Instrument Centre of Sun Yat-Sen University, Guangzhou 510275, PR China

ARTICLE INFO

Article history:
Received 4 June 2008
Available online 14 September 2008

Keywords:
Cationic porphyrin–anthraquinone hybrids
DNA binding
Wavelength-dependent DNA photocleavage

ABSTRACT

Four cationic porphyrin–anthraquinone (Por–AQ) hybrids differing in lengths of flexible alkyl linkage, 5-[4-(1-*N*-anthraquinonon-yl)-L-oxophenyl]-10,15,20-tris(*N*-methylpyridinium-4-yl)porphyrin triiodide, (L = acetyl, pentanoyl, octanoyl, undecanoyl, designed as [AQATMPyP]I_3, [AQPTMPyP]I_3, [AQOTMPyP]I_3 and [AQUTMPyP]I_3, respectively, see Fig. 1), were synthesized and their interactions with DNA were investigated. The results of spectroscopic, denaturation and viscosity measurements suggest that [AQATMPyP]I_3 binds to DNA through non-intercalative mode while the other three hybrids with longer links bind via bis-intercalative mode. Ethidium bromide (EB) competition experiment was carried out to determine the binding constants (K_b) of these compounds for CT DNA, and [AQPTMPyP]I_3 shows the largest K_b among these hybrids. The photocleavage mechanism and wavelength-dependent cleaving abilities of these hybrids to pBR322 plasmid DNA were also comparably investigated.

1. Introduction

Porphyrins take an important part in anti-cancer agents for their unique ability of accumulation in tumor tissues and marked photochemical nuclease activity [1,2]. Cationic porphyrins, represented by *meso*-tetrakis(4-*N*-methylpyridiniumyl)porphyrin (TMPyP), have attracted considerable attention for their additional tight interaction with DNA. TMPyP has been an ideal research model for the DNA-binding agents utilized in photodynamic therapy of tumors [3–6].

On the other hand, another small bioactive molecule, anthraquinone (AQ), is increasingly popular with the development of anthracycline antitumor antibiotics [7–10]. Biochemical evidence suggests that, in common with the anthracyclines, DNA is among the principal cell targets of these drugs. The pharmacological activities of some of these drugs (such as adriamycin and daunomycin) express when a quinone-containing chromophore intercalates into base pairs of the duplex DNA. The intercalative efficiency of drugs to DNA will remarkably influence the pharmacological activity [11–13].

Although adriamycin and daunorubicin are highly efficient antineoplastic agents, their clinical use is limited due to clinical and histopathologic evidence of cardiotoxicity [14–15]. Various efforts have been done to conquer this problem [16–19]. However, since the mechanism of anthracycline cardiotoxicity remains incompletely understood, this problem has not been solved totally. The hope of finding noncardiotoxic yet active anthracycline antitumor antibiotics has spurred the search for new occurring anthracycline and research in synthesizing new quinone-containing analogues. Porphyrins' unique character of high accumulation in the cancer cells gives us the inspiration of designing new Por–AQ hybrid to facilitate the accumulation of drugs in cancer cells and thus decrease the cardiotoxicity of the anthracycline. Among various porphyrins that can link with AQ, cationic porphyrins are preferentially considered for its additional tight intercalation into DNA and thus are expected to enhance the DNA-binding abilities of the drugs additionally.

On the basis of this supposition, we have previously synthesized a cationic Por–AQ hybrid [AQATMPyP]I_3 and investigated its DNA-binding behaviors [20]. However, rather than the expected bis-intercalative mode, it can only partially intercalate into DNA via AQ moiety while its Por moiety binds in an outside binding mode. What's more, the K_b of [AQATMPyP]I_3 was relatively low, even lower than that of the cationic porphyrin parent, 5-(4-hydroxyphenyl)-10,15,20-tris(4-*N*-methylpyridiniumyl)porphyrin

* Corresponding author. Address: MOE Laboratory of Bioinorganic and Synthetic Chemistry, School of Chemistry and Chemical Engineering, Sun Yat-Sen University, No. 135, Xingangxi Road, Guangzhou 510275, PR China. Fax: +86 20 84112245.
E-mail address: ceshjw@163.com (J.-W. Huang).

0045-2068/$ - see front matter © 2008 Elsevier Inc. All rights reserved.
doi:10.1016/j.bioorg.2008.08.002

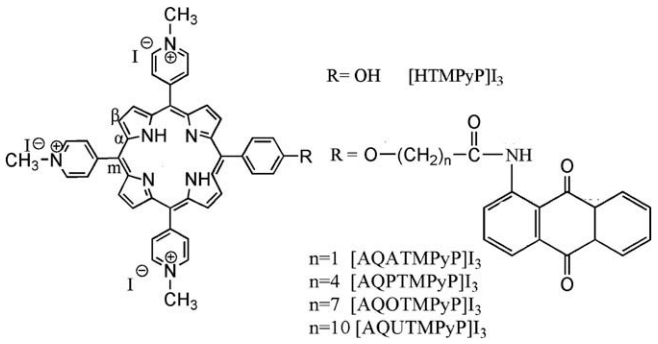

Fig. 1. Structural schematic diagrams of compounds.

triiodide, (namely [HTMPyP]I_3, see Fig. 1). These somewhat disappointing results were mainly attributed to the severe steric hindrance between the AQ and Por planes of [AQATMPyP]I_3 [20].

To remedy the drawback of this unsuccessful work and seek high efficient drugs, herein we have newly synthesized Por–AQ hybrids with longer flexible alkyl links, namely [AQPTMPyP]I_3, [AQOTMPyP]I_3 and [AQUTMPyP]I_3, and compared their DNA-binding properties with [AQATMPyP]I_3. Meanwhile, the DNA photocleavage of these compounds were also comparably investigated. It is expected that the long flexible links will reduce the steric hindrance of these Por–AQ hybrids and thus enhance their DNA-binding and photocleavage efficiencies.

2. Experimental and methods

2.1. Materials

1-Amino-9,10-anthraquinone (Sigma), 5-bromopentanoic acid, 8-bromooctanoic acid, 11-bromoundecanoic acid (Sigma), silica gel (Qingdao) and chloroform (Guangzhou) were commercially available and of analytical grade. CT DNA and pBR322 plasmid DNA were obtained from the Sigma Company. Buffer A (5 mM Tris–HCl, 50 mM NaCl, pH 7.2, Tris = Tris(hydroxymethyl)aminomethane) solution was used in spectral, viscosity and EB competing experiments and buffer B (1.5 mM Na_2HPO_4, 0.5 mM NaH_2PO_4, 0.25 mM Na_2H_2EDTA, pH 7.0, H_4EDTA = *N*,*N*′-ethane-1,2-diylbis[*N*-(carboxymethyl)glycine]) was used for thermal denaturation studies. Gel electrophoresis studies were carried out in buffer C (50 mM Tris–HCl, 18 mM NaCl, pH 7.2). A solution of CT DNA in buffer A gave a ratio of UV absorbance at 260 and 280 nm of 1.85:1, indicating that the CT DNA was sufficiently free of protein [21]. The CT DNA concentration per nucleotide was determined by absorption spectroscopy using the molar absorption coefficient (6600 M^{-1} cm^{-1}) at 260 nm [21].

2.2. Instruments

Element analysis (C, H and N) was carried out with a Perkin-Elmer 240 Q elemental analyzer. ^{1}H NMR spectra were recorded on a Varian-300 spectrometer. All chemical shifts are given relative to tetramethylsilane (TMS). Electrospray Ionization mass spectra (ESI-MS) were recorded on a LCQ DECA XP system (Thremo, USA). UV–vis spectra were recorded on a Perkin-Elmer-Lambda-850 spectrophotometer. Emission spectra were recorded on a Perkin-Elmer Ls55 spectrofluorophotometer. SERS spectra were carried out on a Laser Micro-Raman Spectrometer of Renishaw inVia, with a power of 20 mW at the samples. CD spectra were recorded on a JASCO-J810 spectrometer. Viscosity measurements were carried out with an Ubbelohde viscometer maintained at a constant temperature of 30 ± 0.1 °C in a thermostatic bath. Flow time was measured with a digital stopwatch.

2.3. Measurements

2.3.1. SERS experiment

Ag colloids were prepared by reducing $AgNO_3$ with EDTA according to the reported method [22]. The Ag colloid/compound (or Ag colloid/DNA) SERS-active systems were prepared by mixing equal volume of the compounds (or DNA) solution with the Ag colloid in buffer A to obtain the desired compound or DNA concentrations. In the compound/DNA complex experiments, the solution of DNA was mixed with the Por–AQ hybrid solution at a DNA/compound ratio of 30:1, then an equal volume of the mixed solution was fully mixed with the Ag colloid, and the spectrum was immediately measured at room temperature. The final concentrations of compounds and DNA in all of the SERS-active systems were 5 and 150 μM, respectively.

2.3.2. Equilibrium dialysis experiment

A volume of 100 mL dialysate buffer solution (10 mM sodium phosphate, pH 7.0) containing 50 μM hybrid (c_t) was placed in a conical flask. Extinction coefficient of the Soret band of the hybrid was then spectrophotometrically determined. A 5 mL dialysate buffer solution containing CT DNA (0.5 mM) was pipetted into a dialysis bag, which was then soaked in the 100 mL hybrid solution. The conical flask was then airproofed, and its content was allowed to equilibrate with stirring for 24 h at 25 °C. After the completion of equilibration, the free hybrid concentration (C_f) was determined spectrophotometrically. The amount of bound hybrid (C_b) was determined by the difference, $C_b = C_t - C_f$.

2.3.3. Gel electrophoresis experiment

A pencil-typed high pressure mercury lamp-light filter assembly was used. Yellow light filter was used for visible light ($\lambda > 470$ nm) and purple filter for ultraviolet light ($\lambda < 350$ nm) [23]. The samples were analyzed by electrophoresis for 2.5 h at 80 V in Tris–acetate buffer containing 1% agarose gel. The gel was stained with 1 μg mL^{-1} EB and photographed under UV light.

2.3.4. Cyclic voltammetry (CV) measurements

A three-electrode cell configuration consisting of a platinum working electrode, a silver (Ag^+/Ag) reference electrode, and a platinum auxiliary electrode was used. The supporting electrolyte was 0.1 M tetrabutyl ammonium perchorate (TEAP) buffered at pH 7 which had been N_2 purged for 0.5 h to remove molecular oxygen. The values obtained were normalized with respect to the normal hydrogen electrode (NHE).

2.4. Synthesis

2.4.1. Synthesis of anthraquinone derivates

2.4.1.1. Bromopentanamino-anthraquinone (BrPAAQ). 5-Bromopentanoic acid (10 mmol, 1.5 g) was dissolved in 35 mL of thionyl chloride and the solution was refluxed for 2 h. After cooling to room temperature, thionyl chloride was removed under reduced pressure. Dry benzene (30 mL) was used to wash the residue and then removed. To this residue, a solution of 1-amino-9,10-anthraquinone (5 mmol, 1.1 g) dissolved in dry benzene was added and then the reaction mixture was refluxed for 4 h. The solvent then removed under reduced pressure. BrPAAQ was then gained after washing with 5% Na_2CO_3. Yield: 1.55 g, 90%. ESI-MS *m*/*z* 385.2 ([M−H]$^-$, Calcd for $C_{19}H_{16}BrNO_3$: 385.2).

Bromooctanamino-anthraquinone (BrOAAQ) and Bromoundecanamino-anthraquinone (BrUAAQ) were similarly prepared, replacing 5-bromopentanoic acid by 8-bromooctanoic acid and 11-bromoundecanoic acid, respectively.

BrOAAQ. Yield: 92%. ESI-MS *m*/*z* 427.2 ([M−H]$^-$, Calcd for $C_{22}H_{22}BrNO_3$: 427.2).

BrUAAQ. Yield: 86%. ESI-MS *m*/*z* 469.4 ([M−H]$^-$, Calcd for $C_{22}H_{22}BrNO_3$: 469.4).

2.4.2. Synthesis of Por–AQ hybrids

[HTMPyP]I_3 and [AQATMPyP]I_3 were previously synthesized [20]. The synthetic scheme of Por–AQ hybrids is shown in Scheme 1.

2.4.2.1. [AQPTMPyP]I_3. 5-(4-Hydroxyphenyl)-10,15,20-tris(4-*N*-pyridiniumyl)porphyrin (HTPyP) was synthesized according to the traditional method reported previously [24]. Yield: 4–5%. A mixture of HTPyP (0.45 mmol, 0.286 g), BrPAAQ (0.9 mmol, 0.346 g) and anhydrous K_2CO_3 (0.7 g) in DMF (20 mL) was stirred for 48 h at room temperature. Then the reaction mixture was poured into water (50 mL) and filtered. The crude material was extracted by a mixture of $CHCl_3$–EtOH (25/1, v/v) and purified by chromatography. Evaporation of solvent afforded 5-[4-[(1-*N*-anthraquinonon-yl)pentantyloxophenyl]-10,15,20-tris(4-pyridiniumyl)porphyrin (AQPTPyP) as a purple powder (yield: 0.283 g, 67%). AQPTPyP was then methylated with CH_3I and yielded the cationic porphyrin derivate [AQPTMPyP]I_3 in quantitative yields. Yield: 0.121 g, 92%. (Found: C, 53.38%; H, 4.03%; N, 7.92%. Calcd for $C_{63}H_{51}I_3O_4N_8.3H_2O$: C, 53.33%; H, 4.05%; N, 7.90%.) ESI-MS *m*/*z* 984.1 (M^+, Calcd for $C_{63}H_{51}N_8O_4$: 984.1). ^{1}H NMR (300 MHz, DMSO): chemical shift δ 12.02 (s, 1H, NH–C=O), 9.37(d, *J* = 5.9 Hz, 6H, 2, 6-pyridinium), 9.26 (s, 4H, β-pyrrole), 9.03 (d, J = 6.6 Hz, 4H, β-pyrrole), 8.90 (s, 6H, 3, 5-pyridinium), 8.65 (s, 2H, 2, 6-phenyl), 8.01 (s, 2H, 3, 5-phenyl), 7.80 (s, 4H, AQ-phenyl), 7.08 (s, 2H, AQ-phenyl), 5.09 (s, 1H, AQ-phenyl), 4.73 (s, 9H, N^+–Me), 4.22 (s, 2H, CH_2–O–), 2.24 (s, 2H, CH_2–C=O), 1.18–1.90 (m, 10H, –$(CH_2)_2$–), −3.10 (s, 2H, NH-pyrrole).

[AQOTMPyP]I_3 and [AQUTMPyP]I_3 were similarly prepared, replacing BrPAAQ by BrOAAQ and BrUAAQ, respectively.

[AQOTMPyP]I_3, yield: 87%. (Found: C, 54.90%; H, 4.28%; N, 7.74%. Calcd for $C_{66}H_{57}I_3O_4N_8{\cdot}2H_2O$: C, 54.94%; H, 4.26%; N, 7.77%.) ESI-MS *m*/*z* 1026.4 (M^+, Calcd for $C_{66}H_{57}N_8O_4$: 1026.4). ^{1}H NMR (300 MHz, DMSO): chemical shift δ 11.90 (s, 1H, NH–C=O), 9.49 (d, J = 5.9 Hz, 6H, 2, 6-pyridinium), 9.40 (s, 4H, β-pyrrole), 9.07 (s, 4H, β-pyrrole), 8.94 (d, J = 9.4 Hz, 6H, 3, 5-pyridinium), 8.84 (s, 2H, 2, 6-phenyl), 7.82 (s, 2H, 3, 5-phenyl), 7.67 (t, 4H, AQ-phenyl), 7.36 (d, J = 8.2 Hz, 2H, AQ-phenyl), 5.07 (s, 1H, AQ-phenyl), 4.66 (s, 9H, N^+–Me), 4.26 (s, 2H, –CH_2–O), 2.26 (s, 2H, –CH_2–C=O), 1.18–1.89 (m, 10H, –$(CH_2)_5$–), −3.13 (s, 2H, NH-pyrrole).

[AQUTMPyP]I_3, yield: 87%. (Found: C, 54.42%; H, 4.68%; N, 7.39%. Calcd for $C_{69}H_{63}I_3O_4N_8{\cdot}4H_2O$: C, 54.48%; H, 4.70%; N, 7.37%). ESI-MS *m*/*z* 1068.3 (M^+, Calcd for $C_{69}H_{53}N_8O_4$: 1068.3). ^{1}H NMR (300 MHz, DMSO): chemical shift δ 11.69 (s, 1H, NH–C=O), 9.88 (t, 6H, 2, 6-pyridinium), 9.48 (s, 4H, β-pyrrole), 9.33 (d, J = 6.3 Hz, 4H, β-pyrrole), 8.87 (d, J = 8.2 Hz, 2H, 2, 6-phenyl), 8.56 (s, 6H, 3, 5-pyridinium), 8.13 (s, 2H, 3, 5-phenyl), 7.71 (t, 4H, AQ-phenyl), 7.43 (d, J = 6.5 Hz, 2H, AQ-phenyl), 5.13 (s, 9H, N^+–CH_3), 4.86 (s, 1H, AQ-phenyl), 4.26 (s, 2H, –CH_2–O–), 2.34 (s, 2H, –CH_2–C=O), 1.47–1.81 (m, 16H, –$(CH_2)_8$–), −2.91 (s, 2H, NH-pyrrole).

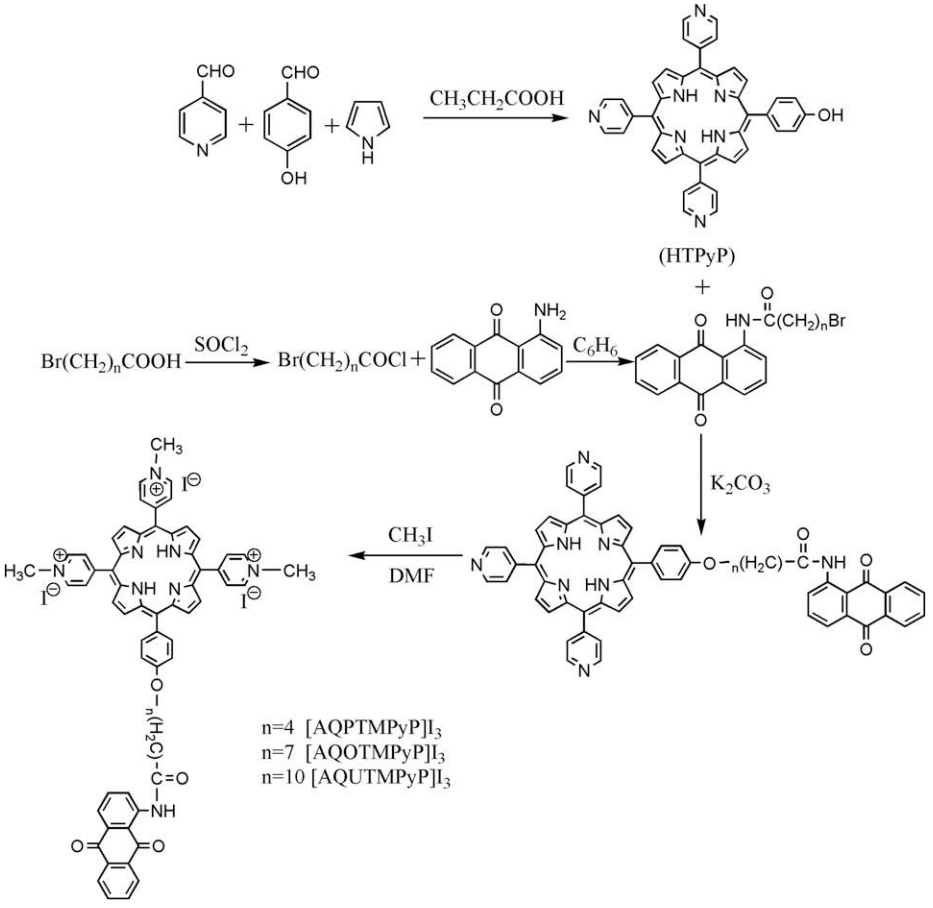

Scheme 1. The synthetic scheme of cationic Por–AQ hybrids.

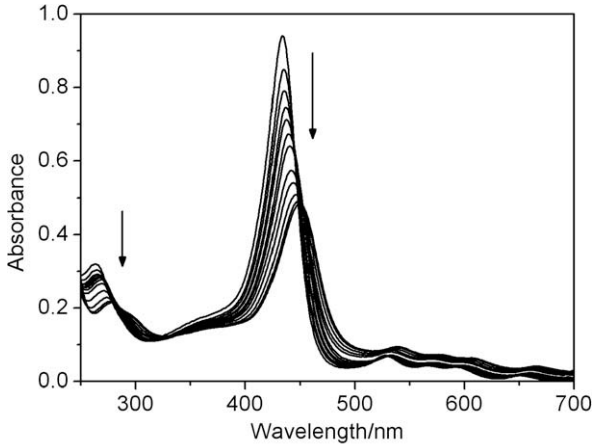

Fig. 2. Absorption spectra of $[AQPTMPyP]I_3$ in buffer A at 25 °C in the presence of increasing amounts of CT DNA. [Por] = 10 μM. Arrows indicate the change in absorbance upon increasing the DNA concentration.

3. Results and discussion

3.1. DNA-binding properties

3.1.1. Absorption titrations

The association of the cationic Por–AQ hybrids with CT DNA was examined by absorption titration in the UV–vis range. Fig. S1 in Supplementary materials shows the absorption spectra of individual AQ (1-amino-9,10-anthraquinone), Por ($[HTMPyP]I_3$) and Por–AQ hybrid ($[AQOTMPyP]I_3$, taken as an example). It is found that Por has an intense absorption band at 400–440 nm (Soret band) and four weak absorption bands from 520 to 680 nm (Q bands). As to AQ, an intense absorption at 240–270 nm is observed. The absorption of the Por–AQ hybrid exhibits not only the Soret band and Q bands of Por, but also the absorption band belongs to AQ moiety.

Fig. 2 exemplifies the absorption spectral changes of $[AQPTMPyP]I_3$ upon DNA addition and those of $[AQOTMPyP]I_3$ and $[AQUTMPyP]I_3$ are available in Fig. S2. Table 1 summarizes the detailed UV titration data. From Fig. 2 and Table 1, one can easily find that with the increasing of DNA concentration, the absorption spectra of the cationic Por–AQ hybrids in the Soret band are remarkably disturbed, with a hypochromism from 46.71% to 52.23% and a bathochromism from 12 to 15 nm. As is well known, the magnitude of spectral perturbation is an intuitional evidence for DNA binding of porphyrins [4]. Intercalation of porphyrin into DNA base pairs is characterized by a red shift (>10 nm) and intensity decrease (up to 40%) in the Soret band of UV–vis spectra; groove binding mode shows no (or minor) change in UV–vis spectra while outside binding mode also exhibits red shift and intensity decrease in the Soret band of porphyrins [4,6,25,26]. Thus, the large degree of hypochromism and bathochromism in the Soret bands of $[AQPTMPyP]I_3$, $[AQOTMPyP]I_3$ and $[AQUTMPyP]I_3$ indicates that the porphyrin moiety of these Por–AQ hybrids binds to DNA in an intercalative binding mode.

Similar phenomena were also observed in the anthraquinone's absorption bands (ranging from 240 to 270 nm) of the UV–vis spectra of these compounds. Upon addition of DNA, the changes of absorption spectra in this range are accompanied by large bathochromism (13 nm for $[AQPTMPyP]I_3$ and $[AQOTMPyP]I_3$, 11 nm for $[AQUTMPyP]I_3$) with substantial hypochromism (36.31%, 35.64% and 35.88% for $[AQPTMPyP]I_3$, $[AQOTMPyP]I_3$ and $[AQUTMPyP]I_3$, respectively). From this large spectral perturbation, we propose that the AQ planes in these hybrids may bind to DNA in a classic intercalative mode. Comparing with the smaller absorption change of $[AQATMPyP]I_3$ [20], it is reasonable if one considers that the longer flexible chains decrease the steric hindrance between Por and AQ planes and are favorable for the bis-intercalating of these hybrids to DNA.

3.1.2. Fluorescence studies

Fluorescence titration experiments of the compounds with CT DNA were performed and the results are shown in Figs. 3 and S3. It is found that the fluorescence intensities of these hybrids at the Por's and AQ's characteristic emission bands (ca. 665 and 370 nm, respectively) are remarkably enhanced upon the addition of DNA. Since the hydrophobic environment provided by DNA can protect the compound from quenching by water molecules, the emission increase is widely admitted as an indication of the interaction between drugs and DNA [4–6,25,26]. Thus, the significant increases in both Por's and AQ's emission ranges suggest that both two moieties in the hybrids interact with DNA rather strongly.

It is interesting to find that a new emission peak centered at ca. 600 nm appears and increases with the addition of DNA. This peak can be attributed to the Por monomers which result from the

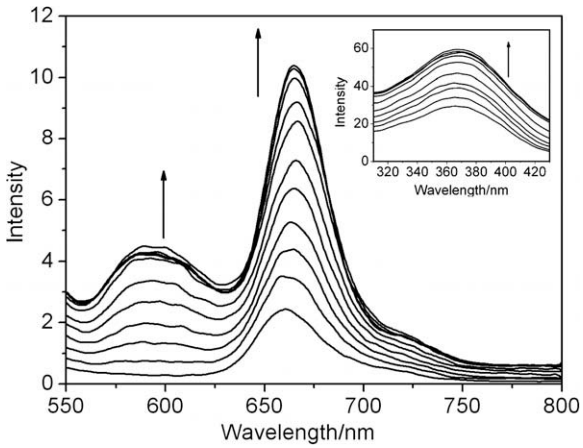

Fig. 3. Emission spectra for Por moiety of $[AQPTMPyP]I_3$ in the absence and presence of CT DNA in buffer A. Insert: the emission spectra for AQ moiety of $[AQPTMPyP]I_3$. [Por] = 10 μM. Arrows show the intensity change upon increasing DNA concentrations. λ_{ex} = 449 nm for the Por moiety and 280 nm for AQ moiety.

Table 1
Physical data of Por–AQ hybrids binding with CT DNA

Compound	UV–vis spectra				Fluorescence spectra		ICD spectra		ΔT_m (°C)	K_b ($\times 10^6$ M^{-1})
	Por		AQ		Por	AQ	Por			
	$\Delta\lambda$ (nm)	H%	$\Delta\lambda$ (nm)	H%	Increase%		+	–		
$[AQPTMPyP]I_3$	15	52.23	13	36.31	403	133		447	12.8	8.5
$[AQOTMPyP]I_3$	12	49.31	13	35.66	311	119		445	10.1	7.4
$[AQUTMPyP]I_3$	13	46.71	11	35.88	238	83	415	444	8.9	6.8

breaking of Por aggregation by DNA molecules [27,28]. The subsequent interaction of these Por monomers with DNA is another reason for the increase of this peak.

Steady-state emission quenching experiment using potassium ferrocyanide ($K_4Fe(CN)_6$) as a quencher was frequently employed to evaluate the DNA binding of positively charged compounds. Fig. 4a gives [AQPTMPyP]I_3 as an example to illustrate the quenching effect of $K_4Fe(CN)_6$ on the fluorescence intensities of compound in the absence and presence of CT DNA. From Fig. 4a, we can find that in the absence of CT DNA, the weak fluorescence of [AQPTMPyP]I_3 is completely quenched at the initial stage of $K_4Fe(CN)_6$ addition. However, in the DNA–drug system, there is no substantial change on the fluorescence intensity of [AQPTMPyP]I_3 with increasing $K_4Fe(CN)_6$ concentrations. This behavior may be explained by the repulsion of the highly anionic $[Fe(CN)_6]^{4-}$ by the DNA polyanion which hinders the bound compound from quenching of the emission. Similar results were obtained in the case of [AQOTMPyP]I_3 and [AQUTMPyP]I_3. Fig. 4b shows plots of $K_4Fe(CN)_6$ emission quenching on these hybrids. It is widely admitted that the slope of the quenching plot reflects different accessibilities of cations to DNA and a smaller slope corresponds to better DNA protection and stronger binding affinity [29]. The slopes of the plots in Fig. 4b are all near to zero, suggesting that all these compounds can bind to the DNA rather strongly.

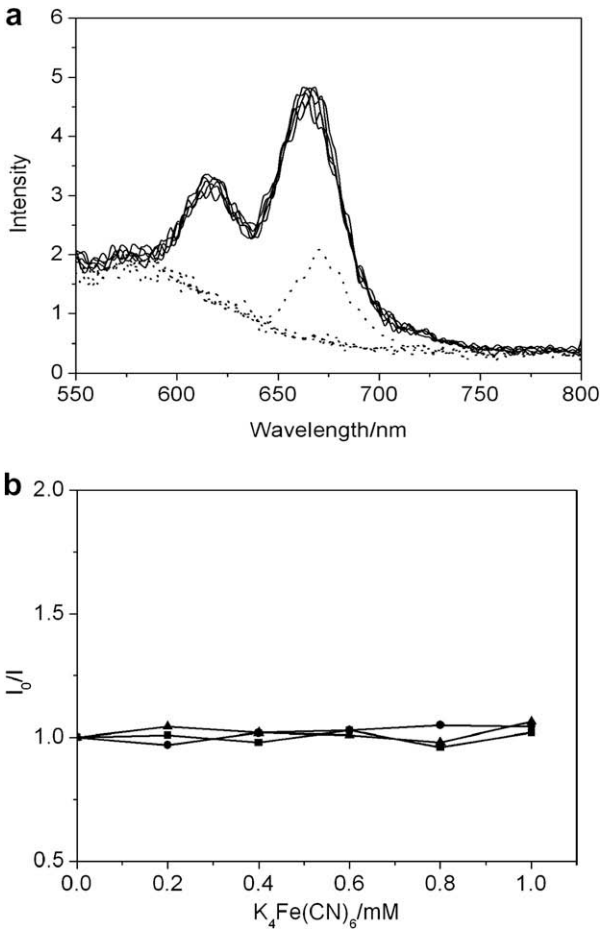

Fig. 4. (a) Emission quenching with $K_4Fe(CN)_6$ for free (dot line) and DNA-bound (solid line) [AQPTMPyP]I_3; (b) $[Fe(CN)_6]^{4-}$ quenching plot for DNA-bound [AQPTMPyP]I_3 (■), [AQOTMPyP]I_3 (●) and [AQUTMPyP]I_3 (▲) in buffer A. I_0 and I are the fluorescence intensities of the compounds in the absence and presence of $K_4Fe(CN)_6$. [Por]/[DNA] = 0.25.

3.1.3. SERS investigation

SERS is a powerful tool for the study of the interactions of drugs, especially fluorescence molecules, with biomacromolecules at very low concentrations. The metal colloids can be adapted for the application in the study of biological objects, because they do not modify to a great extent the structures of biological molecules adsorbed on their surface [30]. To further clarify the binding modes of these cationic Por–AQ hybrids to CT DNA, SERS spectra were measured.

The SERS spectra of the hybrids in the absence and presence of CT DNA are shown in Fig. 5. Table 2 summarized the main SERS bands of the compounds and their assignments. Fig. 5 also exhibited the SERS spectrum of free CT DNA. It is found that no substantial SERS signal is given by free CT DNA, since the Ag colloids have negative charges on their surface, which repulses the adsorption of negative-charged DNA molecules [31].

Curves a–d in Fig. 5 show the SERS spectra of the compounds in the absence of DNA, which are very similar to each other. This similarity in the SERS spectra results from the quite similar molecular structure of these compounds. Curves a′–d′ in Fig. 5 show the SERS spectra of complexes of Por–AQ hybrids at 5 μM with CT DNA at 150 μM. SERS spectra of these compounds in the presence of DNA are also quite similar to each other but very different from those in the absence of DNA. Most bands of the compound/DNA complexes disappear, indicating that the interactions of Por–AQ compounds with DNA can largely reduce the amount of compounds adsorbed on Ag colloids [31]. Especially, the band at 330 cm^{-1} is mainly assigned to the bending vibration of Por ring and is the marker band of the free-base Por compounds in the SERS-active system; the disappearance of this band is due to the vanishment of free-base Por molecules surrounding Ag colloids after the interaction between Por–AQ compounds and DNA

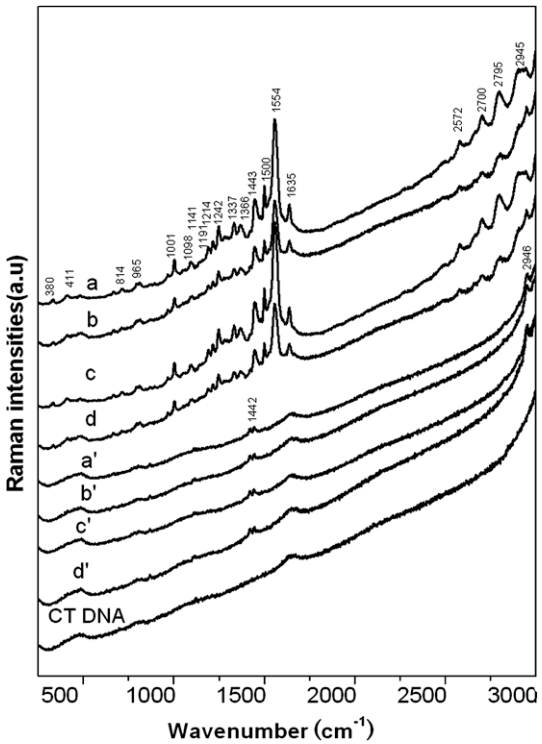

Fig. 5. SERS spectra (250–3000 cm^{-1}) of CT DNA and Por–AQ hybrids in the absence (a–d) and presence (a′–d′) of CT DNA. (a)–(d) for free [AQATMPyP]I_3, [AQPTMPyP]I_3, [AQOTMPyP]I_3 and [AQUTMPyP]I_3, respectively; (a′)–(d′) for DNA complexes with [AQATMPyP]I_3, [AQPTMPyP]I_3, [AQOTMPyP]I_3 and [AQUTMPyP]I_3, respectively. [DNA]/[Por] = 30:1.

Table 2
Raman frequencies and assignments for Por–AQ hybrids[a]

Raman shift (cm^{-1})	Assignments[b]	Raman shift (cm^{-1})	Assignments[b]
330	δ(por)	1242	$\nu(C_m–pyr)$
411	δ(por) + ν(Ag–N)	1337	$\nu_s(N–C_\alpha)$
814	pyr $\nu(N^+–CH_3)$	1443	$\nu_s(CH_2)$
	δ_s(por)	1500	$\nu_s(C_{14}–N_{15})$
965	$\nu(C_\alpha–C_\beta)$	1554	ν(AQ)
1001	$\nu(C_m–C_\alpha)$	1635	δ(pyr) + ν_s(C=O)
1098	$\delta_s(C_\beta–H)$	2572	ν(C–H)
1141	$\nu(C_\alpha–N)$	2700	$\nu(C–O_{12})$
1191	δ(pyr), $\nu(N^+–CH_3)$	2795	$\nu_s(CH_2)$
1214	δ(pyr), $\nu(C_\alpha–N)$	2945	$\nu(CH_2)$

[a] Band assignments are according to Refs. [31–34].
[b] *Abbreviations:* ν, stretching mode; δ, bending mode; *s*, symmetric mode; pyr, *N*-methylpyridinium; por, porphyrin core.

[31–33]. The vanishment of bands centered at 411, 814, 965, 1001, 1098, 1141 nm which are attributed to Por, also indicates the Por moieties of the compounds are protected by DNA from adsorbing on Ag particles. The band at 1554 cm^{-1} which is the characteristic band of anthracene compounds vanishes [34], indicating that the AQ moieties of the compounds are embedded in DNA molecules. However, the remaining of bands centered at 1442, 2946 nm, which can be ascribed to the carbon links in the molecule, suggests that the flexible carbon links may be still exposed in the solvent when the two planar moieties are well protected by DNA. In summary, all of these changes in the SERS intensities are ascribed to the intense interactions between the Por–AQ hybrids and DNA.

Moreover, the chosen protocol for the SERS sample preparation allows the DNA–compound adduct to be formed before its addition to the colloid solution (see Section 2). Consequently, the spectral changes confirm that the cationic Por–AQ hybrids efficiently bind to DNA even in Ag sols. In this medium, the preference of cationic compound for polyanionic DNA prevails over negatively charged Ag nanoparticles. This also reveals the high binding affinities between the cationic drugs and DNA [35].

3.1.4. ICD spectra

It has been reported that the ICD spectra in the Soret region of Por are well-defined indicators for the binding modes toward DNA: a positive ICD peak is due to groove binding; a negative ICD peak is due to intercalative binding; a conservative ICD peak is ascribed to the outside binding of Por to DNA [4,6,25].

Fig. 6 illustrates the ICD spectra and Table 1 lists physical data of the Por derivatives bound to CT DNA. None of these compounds as well as DNA by themselves displays any CD spectra signal in the visible region, but ICD spectra were observed in the Soret band of these compounds with DNA titration. The ellipticities observed for [AQPTMPyP]I_3 and [AQOTMPyP]I_3 in the presence of DNA are predominantly negative in character and centered at the wavelength ranging from 430 to 470 nm. With the addition of DNA, the negative signal of ICD spectra becomes stronger. Since the negative ICD signal is diagnostic of intercalative binding, this result confirms that the Por moieties of [AQPTMPyP]I_3 and [AQOTMPyP]I_3 intercalate into the DNA duplex under the experimental conditions. The ICD signal of [AQUTMPyP]I_3 is also dominantly negative with exception of a rather weak positive band around 415 nm at higher DNA concentration, suggesting that the DNA-binding mode of its Por moiety is primarily intercalation accompanied by groove binding at high [DNA]/[Por] ratio. On the contrary, the substantial conservative ICD signal of [AQATMPyP]I_3 evidences that its Por moiety binds to DNA in outside binding mode [20]. The distinct ICD signals of these compounds are in good consistent with foregoing experimental results. It is likely that, rather than suffer severe steric hindrance from each other, the Por and AQ moieties in the Por–AQ compounds with longer flexible bridging links could interact with DNA independently, and both are sterically appropriate to bind with DNA in intercalative mode.

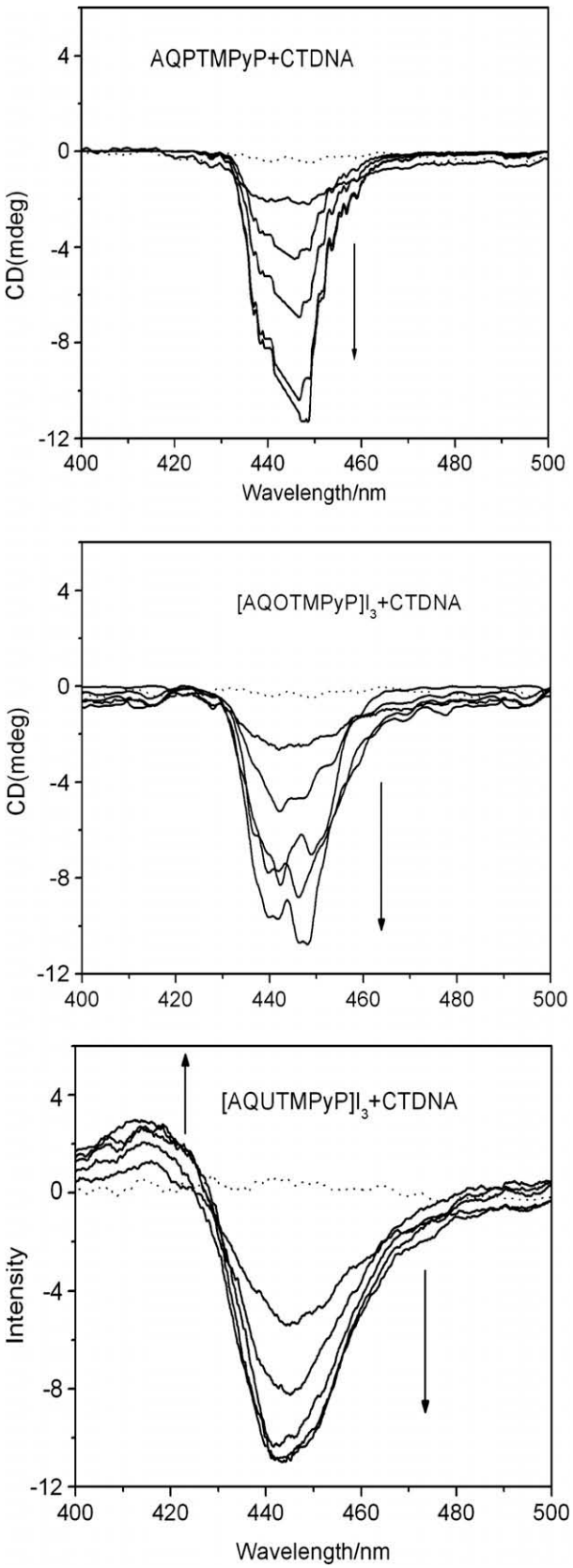

Fig. 6. ICD spectra of Por–AQ hybrids in the absence (dot line) and presence (solid line) of CT DNA in buffer A. [Por] = 10 μM. [Por]/[DNA] = 0.3, 0.2, 0.15, 0.10, 0.05. Arrows indicate the change in ICD spectra upon increasing the DNA concentration.

3.1.5. Thermal denaturation studies

The thermal denaturation of double-helical polynucleotides from double stranded to single stranded is manifested as hyperchromism in the UV absorption. The melting temperature (T_m) of DNA is sensitive to its double-helix stability and the binding of compounds to DNA alters the T_m value, with dependence on the strength of the interactions [3]. Upon binding of small molecules to DNA, the T_m value of the B-form DNA should become higher, as compared to that of unbound or free DNA. In addition, as the small molecules bind more strongly to the DNA, the increase in the T_m value will become larger. Therefore, the T_m value can be used as an indicator of the binding properties and binding strengths of compounds with DNA. Meanwhile, it has been proved that T_m will considerably increase when intercalation binding mode occurs [4,36].

The melting curves of CT DNA in the absence and presence of compounds are presented in Fig. 7. Under the present experimental conditions, the melting curve has a transition, and the T_m value of free double-stranded CT DNA is 60.6 ± 0.2 °C; When mixed with the compounds, the observed melting temperatures of CT DNA increase to different extents and the increases of T_m (ΔT_m) are summarized in Table 1.

From Table 1, we can find that the values of ΔT_m in the presence of $[AQPTMPyP]I_3$, $[AQOTMPyP]I_3$ and $[AQUTMPyP]I_3$ are relatively large, (12.4, 10.1 and 8.9 °C, respectively), suggesting that the compounds may interact with DNA in an intercalative mode and have strong DNA-binding affinities. These increases are much larger than that of $[AQATMPyP]I_3$ (4.6 °C), which can be understood by the non-intercalative binding mode of $[AQATMPyP]I_3$ to DNA [20]. Moreover, it is surprising that the increase about $[AQPTMPyP]I_3$, $[AQOTMPyP]I_3$ and $[AQUTMPyP]I_3$ are even larger than that of $[HTMPyP]I_3$ (7.7 °C), which has been proved to intercalate into DNA through its porphyrin plane [20]. It is reasonable if one concludes from this result that besides the perfect DNA intercalation of Por moieties, the AQ planes in the Por–AQ hybrids intercalate into DNA duplex, too. Thus, the results of thermal denaturation further argue for the bis-intercalative DNA-binding mode of these compounds.

3.1.6. Viscosity analysis and equilibrium dialysis

In the absence of X-ray structural data, hydrodynamic methods which are sensitive to changes in the length of DNA are arguably the most critical test of the classical intercalation model, and therefore they provide the most definitive means of inferring the binding mode of DNA in solution [4]. Intercalation mode is expected to lengthen the DNA helix as the base pairs are pushed apart to accommodate the bound ligand, leading to an increase in the DNA viscosity. In contrast, a partial, non-classical intercalation of ligand could bend (or kink) the DNA helix and reduce its effective length and, concomitantly, its viscosity. When outside binding or groove binding occurs, the viscosity of DNA will not change basically [3,4,37].

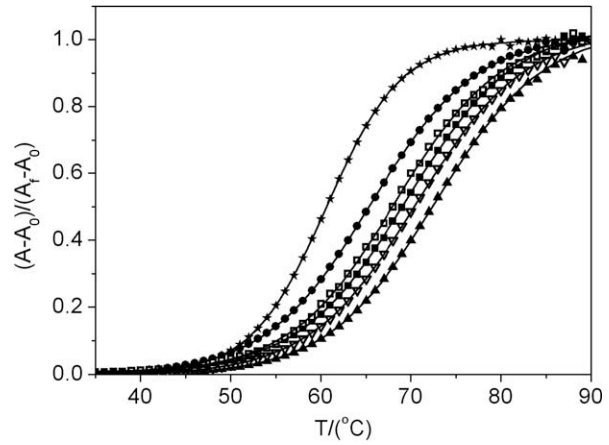

Fig. 7. Melting curves of CT DNA at 260 nm in the absence (*) and the presence of $[HTMPyP]I_3$ (□), $[AQATMPyP]I_3$ (●), $[AQPTMPyP]I_3$ (▲), $[AQOTMPyP]I_3$ (▽) and $[AQUTMPyP]I_3$ (■) in buffer B. [Por] = 10 μM, [DNA] = 100 μM.

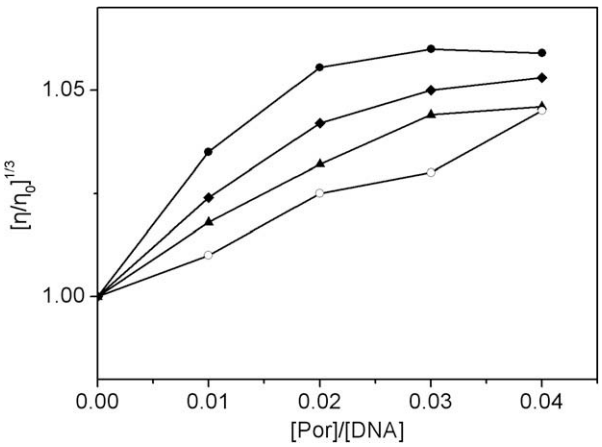

Fig. 8. Plots of the relative viscosity change of CT DNA in the presence of $[HTMPyP]I_3$ (○), $[AQPTMPyP]I_3$ (●), $[AQOTMPyP]I_3$ (♦) and $[AQUTMPyP]I_3$ (▲) in buffer A at 30 ± 0.1 °C. [DNA] = 0.5 mM. η is the viscosity of DNA in the presence of the compounds and η_0 is the viscosity of DNA alone.

The viscosity of the buffer solutions of CT DNA increases with the addition of the compounds, $[AQPTMPyP]I_3$, $[AQOTMPyP]I_3$ and $[AQUTMPyP]I_3$ (Fig. 8). Such an increase provides striking evidence for the intercalation of these hybrids into the DNA duplex. Moreover, it is surprising that the increase degrees of these Por–AQ hybrids are even larger than that of $[HTMPyP]I_3$. This interesting result is believed to be caused by the DNA intercalation of AQ moieties in these hybrids, as has been demonstrated in thermal denaturation studies. Thus, the bis-intercalation of $[AQPTMPyP]I_3$, $[AQOTMPyP]I_3$ and $[AQUTMPyP]I_3$ to DNA is further, definitively proved by the viscosity results here.

Attempts to see the DNA viscosity change at higher drug concentrations for the cationic Por–AQ hybrids cannot be successful because red precipitations were observed visually under these conditions. This phenomenon is common in the viscosity research of cationic porphyrins with DNA and can be ascribed to the external binding mode between the positive macrocycles and the negative phosphate backbone [38]. Equilibrium dialysis experiments were thus carried out to investigate the DNA-binding behaviors of these compounds at a [Por]/[DNA] ratio of 0.1 and the results are summarized in Fig. 9 as a histogram. As shown in Fig. 9, under identical experimental conditions, the amounts of the hybrids bound to CT DNA decreased in the order of $[AQPTMPyP]I_3$ > $[AQOTMPyP]I_3$ > $[AQUTMPyP]I_3$ > $[AQATMPyP]I_3$. This order is in good agreement with the results of absorption titration and thermal denaturation studies above and should be closely correlated with their DNA-binding affinities [39].

3.1.7. Competitive binding experiments

The above experimental results suggest that there are some interactions between these compounds and DNA. In order to compare quantitatively, their binding constants (K_b) to CT DNA have to be measured. UV–vis titration has several limitations in dealing with this kind of compounds and fluorescence spectra were thus used to measure K_b of these hybrids by competition with EB to bind with DNA [20,40,41].

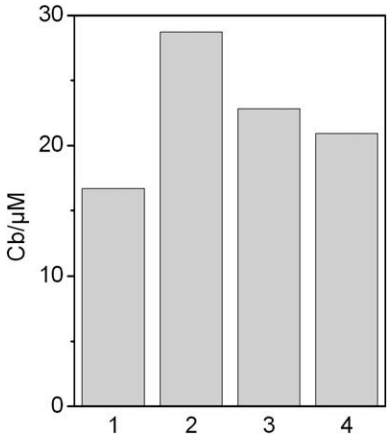

Fig. 9. The amounts of Por–AQ hybrids bound to CT DNA (C_b) in dialysate buffer (10 mM sodium phosphate, pH 7.0). Columns 1, 2, 3, 4 for [AQATMPyP]I_3, [AQPTMPyP]I_3, [AQOTMPyP]I_3 and [AQUTMPyP]I_3, respectively. [DNA] = 0.5 mM, C_t = 50 μM, dialyse for 24 h at 25 °C.

The EB competitive binding experiments were carried out and quenching plots are given in Fig. 10. The quenching plots of I_0/I vs [Por]/[DNA] are in good agreement with the linear Stern–Volmer equation with slopes of 5.32, 4.65, 4.26 for [AQPTMPyP]I_3, [AQOTMPyP]I_3 and [AQUTMPyP]I_3, respectively. We can also learn from Fig. 10 that 50% of EB molecules were replaced from DNA-bound EB at a concentration ratio of [Por]/[EB] = 1.17, 1.35 and 1.47 for [AQPTMPyP]I_3, [AQOTMPyP]I_3 and [AQUTMPyP]I_3, respectively. By taking K_b of 1.0×10^7 M^{-1} for EB under this experimental condition [42], the K_b of [AQPTMPyP]I_3, [AQOTMPyP]I_3 and [AQUTMPyP]I_3 were derived 8.5×10^6, 7.4×10^6 and 6.8×10^6 M^{-1} (K_b(EB)/1.17, K_b(EB)/1.35 and K_b(EB)/1.47), respectively [43]. The DNA-binding affinities of the Por–AQ hybrid with longer bridging links are much higher than that of [AQATMPyP]I_3 (3.44×10^6 M^{-1}) [20]. This can be explained by the fact that both two moieties in the long-linked hybrids intercalate into DNA and both can replace EB from DNA helix, leading to relatively high binding affinities.

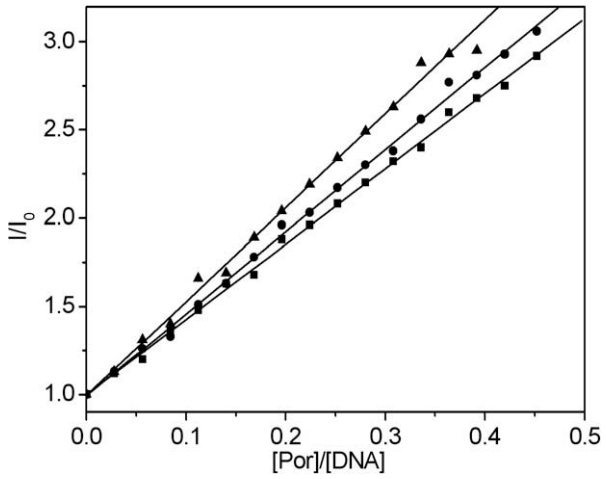

Fig. 10. Fluorescence quenching plots of DNA-bound EB by [AQPTMPyP]I_3 (▲), [AQOTMPyP]I_3 (●) and [AQUTMPyP]I_3 (■) in buffer A. [DNA] = 100 μM, [EB] = 16.0 μM, λ_{ex} = 537 nm.

From the foregoing experimental researches on DNA-binding mode and affinity, it can be stated that the stereochemistry, especially the length of flexible linkage between the two planes, significantly influences the binding behaviors of these cationic water-soluble Por–AQ hybrids to DNA.

3.2. DNA photocleavage

3.2.1. Mechanism of DNA photocleavage

Thermodynamic considerations play a key role in assessing the likelihood that excited quinone compounds will react with DNA by electron transfer (ET) [44,45]. Weller equation [46] is widely used to determine whether the reaction is feasible:

$$\Delta G_{et} = E^{+}_{D/D} - \Delta E_{0,0} - E^{-}_{A/A}$$

The oxidation potentials of the nucleic acid bases have been previously determined [47]. Guanine has the lowest oxidation potential (1.29 V, $E^{+}_{D/D}$) among the bases and may have lower value in DNA since there is GG staking [48]. The reduction potentials of these Por–AQ compounds ($E^{-}_{A/A}$) were determined using CV method (see results in Table 3 and Supplementary materials, Fig. S4) and the $\Delta E_{0,0}$ energies were calculated from their maximum emission wavelength (λ_{em}) [49]. ΔG_{et} were calculated according to the Weller equation and the results are listed in Table 3. From Table 3, we can find that the values of ΔG_{et}, (−0.25, −0.28 and −0.23 eV for [AQPTMPyP]I_3, [AQOTMPyP]I_3 and [AQUTMPyP]I_3, respectively) are relatively low, revealing that electron transfer from guanine of DNA to the Por–AQ hybrids is exothermic and therefore feasible on thermodynamic grounds.

On the other hand, the mechanism of DNA photocleavage by the porphyrin moiety was investigated in the presence of different potentially inhibiting agents. The results are given in Figs. 11 and S5. Similar cases were observed for all the hybrids. It is found that in the presence of the hydroxyl radical scavengers (ethanol, methanol and DMSO), percentages of Form II DNA were not significantly affected, suggesting that the hydroxyl radical is hardly involved in the DNA photocleavage by these hybrids. However, the percentages of Form II DNA after photoirradiation were decreased by the addition of NaN_3, which is known to be a scavenger of $^1O_2$ [50]. When the sample solutions were thoroughly degassed with Ar and maintained under Ar atmosphere during the experiment, the DNA photocleavage was greatly inhibited as compared with that in air. In addition, the photocleavage ability was substantially enhanced by replacing the reaction media H_2O by 70% D_2O which makes the life span of $^1O_2$ longer. These results suggest that the pathway to produce Form II DNA is aerobic and $^1O_2$ are the reactive species responsible for the DNA photocleavage by these hybrids.

The experimental protocol used here is useful in the preliminary evaluation of the mechanism of DNA photocleavage, although it lacks the accuracy to elucidate the mechanism of DNA photocleavage in some respects [51]. Therefore, these conclusions will have to be checked by a more precise protocol with the use of end-labeled oligodeoxynucleotides in the future [52].

Table 3
The reduction potentials (E^{-}_{A/A^-}), ΔE energies and ΔG_{et} of the compounds

	E^{-}_{A/A^-} (V, vs Ag^+/Ag)	E^{-}_{A/A^-} (V, vs NHE)	λ_{em} (nm)	ΔE (eV)	ΔG_{et} (eV)
[AQPTMPyP]I_3	−1.02	−0.34	660	1.88	−0.25
[AQOTMPyP]I_3	−0.98	−0.30	661	1.87	−0.28
[AQUTMPyP]I_3	−1.01	−0.33	669	1.85	−0.23

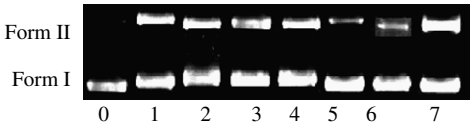

Fig. 11. Photocleavage of pBR322 plasmid DNA in the presence of $[AQPTMPyP]I_3$ and different inhibitors after irradiation by visible light ($\lambda > 470$ nm) for 15 min. Ten-microliters reaction mixtures contained 1.0 μg of plasmid DNA in buffer C. [Por] = 2 μM. Lane 0: DNA control; lane 1: in the presence of porphyrin, no inhibitor; lanes 2–6: in the presence of porphyrin and inhibitor: (2) ethanol (5 mM), (3) methanol (5 mM), (4) DMSO (5 mM); (5) NaN_3 (5 mM), (6) under an Ar atmosphere, (7) 70% D_2O.

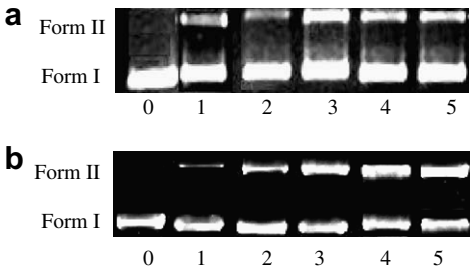

Fig. 12. Photocleavage of pBR322 plasmid DNA after irradiated by visible light ($\lambda > 470$ nm) in air (a) or ultraviolet light ($\lambda < 350$ nm) under an Ar atmosphere (b). Ten-microliters reaction mixtures contained 1.0 μg of plasmid DNA in buffer C. [Por] = 2 μM. Lane 0: untreated DNA, no irradiation; Lanes 1, 2, 3, 4, 5: in the presence of $[HTMPyP]I_3$, $[AQATMPyP]I_3$, $[AQPTMPyP]I_3$, $[AQOTMPyP]I_3$ and $[AQUTMPyP]I_3$, respectively, irradiation for 20 min.

3.2.2. Wavelength-dependent DNA photocleavage

To investigate the photocleavage ability of Por and AQ moiety of the hybrid, respectively, wavelength-dependent experiments were carried out by irradiating with visible light (at porphyrin's excited wavelength) or UV light (at anthraquinone's excited wavelength). The results are given in Fig. 12. Without irradiation, no substantial cleavage of DNA was observed for all the compounds (data not shown). Under irradiation with visible light, the DNA-photocleavage activities of the cationic Por–AQ hybrids follow an order of $[AQPTMPyP]I_3 > [AQOTMPyP]I_3 > [AQUTMPyP]I_3$ ($>[HTMPyP]I_3$) > $[AQATMPyP]I_3$) which is in parallel with the magnitude of their DNA-binding constants (K_b). It seems that large K_b and intercalative binding mode are advantageous to effective DNA photocleavage. These results are in high consistent with previous reports on the relationship between DNA-binding and photocleavage of cationic porphyrins [50,52].

The UV light irradiation experiment was carried out in Ar atmosphere to get rid of the possible effect of Por moiety. The results shows that the DNA-photocleavage abilities of $[AQPTMPyP]I_3$, $[AQOTMPyP]I_3$ and $[AQUTMPyP]I_3$ are similar and higher than that of $[AQATMPyP]I_3$. This may also result from the more effective DNA binding of AQ moieties in the long-linked hybrids than that in $[AQATMPyP]I_3$.

4. Conclusion

This paper and its predecessor [20] introduced a series of cationic Por–AQ hybrids with various bridging links and their binding behaviors with CT DNA as well as their photocleavage activities to plasmid DNA. Through spectral, thermodynamic and hydrodynamic methods, it is found that the Por and AQ units in $[AQPTMPyP]I_3$, $[AQOTMPyP]I_3$ and $[AQUTMPyP]I_3$ are sterically appropriate to bis-intercalation while those of $[AQATMPyP]I_3$ suffer from severe steric strains in binding with DNA (see Fig. 13). All the cationic water-soluble Por–AQ derivatives give rise to DNA photocleavage

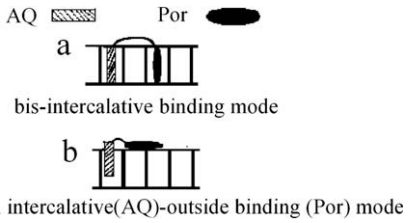

Fig. 13. The binding modes of cationic Por–AQ hybrids to CT DNA: (a) for $[AQPTMPyP]I_3$, $[AQOTMPyP]I_3$ and $[AQUTMPyP]I_3$; (b) for $[AQATMPyP]I_3$.

and serve as wavelength-dependent photonucleases under irradiation with visible and ultraviolet light. The order of efficiency for DNA binding and photocleavage is $[AQPTMPyP]I_3 > [AQOTMPyP]I_3 > [AQUTMPyP]I_3 > [AQATMPyP]I_3$. Proper length of flexible linkage seems very significant in designing such kind of drugs with multiple interactive sides. These results may facilitate the design of highly-efficient yet noncardiotoxic anthracycline antitumor antibiotics.

Acknowledgments

We are grateful to the supports of Guangzhou Municipality Science and Technology Bureau of China, the National Natural Science Foundation of China and National Key Foundation Research Development Project (973) Item of China (No. 2007 CB815306).

Appendix A. Supplementary data

Supplementary data associated with this article can be found, in the online version, at doi:10.1016/j.bioorg.2008.08.002.

References

[1] T.J. Dougherty, Y. Hayata, Cancer Res. 41 (1981) 4606–4612.
[2] S.I. Umemura, Cancer Res. 84 (1993) 582–588.
[3] R.J. Fiel, J.C. Howard, E.H. Mark, N.D. Gupta, Nucleic Acids Res. 6 (1979) 3093–3118.
[4] R.F. Pasternack, E.J. Gibbs, J.J. Villafranca, Biochemistry 22 (1983) 2406–2414.
[5] D.R. McMillin, K.M. McNett, Chem. Rev. 98 (1998) 1201–1220.
[6] D.R. McMillin, A.H. Shelton, S.A. Bejune, P.E. Fanwick, R.K. Wall, Coord. Chem. Rev. 249 (2005) 1451–1459.
[7] D.T. Breslin, J.E. Coury, J.R. Anderson, L. Mcfail-Isom, Y. Kan, L.D. Williams, L.A. Bottomley, G.B. Schuster, J. Am. Chem. Soc. 119 (1997) 5043–5044.
[8] R.E. McKnight, J.G. Zhang, D.W. Dixon, Bioorg. Med. Chem. Lett. 14 (2004) 401–404.
[9] G.S.B. Vernon, J. Mol. Graph. Model. 26 (2007) 14–19.
[10] P. Wardman, Clin. Oncol. 19 (2007) 397–417.
[11] A. DiMarco, R. Silverstrini, M. Soldati, P. Orezzi, T. Dasdia, B.M. Scarpinato, L. Valentini, Nature 201 (1964) 706–707.
[12] Y.K. Liaw, V.M. Li, J.H. Boom, A.H. Wang, Proc. Natl. Acad. Sci. USA 88 (1991) 4845–4849.
[13] K. Atsushi, G. Tomoko, N. Shigeo, I. Toshihiro, T. Makoto, Chem. Lett. 30 (2001) 370–373.
[14] M.M. Ali, E. Frei, J. Straub, A. Breuer, M. Wiessler, Toxicology 179 (2002) 85–93.
[15] T. Simunek, I. Klimtová, J. Kaplanová, M. Stěrba, Y. Mazurová, M. Adamcoá, R. Hrdina, V. Gersl, P. Ponka, Pharmacol. Res. 51 (2005) 223–231.
[16] H.N. Abramson, J.W. Banning, J.P. Nachtman, M.S. Roginski, H.C. Wormser, J.Z. Wu, R.R. Schroeder, M.M. Bernardo, J. Med. Chem. 29 (1986) 1709–1714.
[17] S. Christiansen, J.J. Stypmann, U.R. Jahn, K. Redmann, M. Fobker, A.D. Gruber, H.H. Scheld, D.J. Hammel, J. Heart Lung Transplant. 22 (2003) 301–308.
[18] M.P. Cole, L. Chaiswing, T.D. Oberley, S.E. Edelmann, M.T. Piascik, S.M. Lin, K.K. Kiningham, D.K. StClair, Cardiovasc. Res. 69 (2006) 186–197.
[19] J.O.B. Peter, Toxicology 245 (2008) 206–218.
[20] P. Zhao, L.C. Xu, J.W. Huang, K.C. Zheng, J. Liu, H.C. Yu, L.N. Ji, Biophys. Chem. 134 (2008) 72–83.
[21] M.E. Reichmann, S.A. Rice, C.A. Thomas, P. Doty, J. Am. Chem. Soc. 76 (1954) 3047–3053.
[22] J. Chen, J.M. Hu, Z.S. Xu, R.S. Sheng, Appl. Spectrosc. 47 (1993) 292–295.
[23] C.J. Sansonetti, M.L. Salit, J. Reader, Appl. Opt. 35 (1996) 74–77.
[24] C. Casas, B. Saint-Jalmes, C. Loup, C.J. Lacey, Bernard Meunier, J. Org. Chem. 58 (1993) 2913–2917.
[25] J.S. Trommel, L.G. Marzilli, Inorg. Chem. 40 (2001) 4374–4383.
[26] L.N. Ji, X.H. Zou, J.G. Liu, Coord. Chem. Rev. 216–217 (2001) 513–536.

[27] M. Tabata, A.K. Sarker, E. Nyarko, J. Inorg. Biochem. 94 (2003) 50–58.
[28] E. Nyarko, A. Habib, M. Tabata, Inorg. Chim. Acta 357 (2004) 739–745.
[29] C.V. Kumar, J.K. Barton, N.J. Turro, J. Am. Chem. Soc. 107 (1985) 5518–5523.
[30] J. De Groot, R.E. Hester, J. Phys. Chem. 91 (1987) 1693–1696.
[31] C.Y. Wei, G.Q. Jia, J.L. Yuan, Z.C. Feng, C. Li, Biochemistry 45 (2006) 6681–6691.
[32] M. Procházka, P.Y. Turpin, J. Sÿtěpánek, J. Bok, J. Mol. Struct. 482–483 (1999) 221–224.
[33] S.N. Terekhov, S.G. Kruglik, V.L. Malinovskii, V.A. Galievsky, V.S. Chirvony, P.Y. Turpin, J. Raman Spectrosc. 34 (2003) 868–881.
[34] Y.C. Ning, Structure Identification of Organic Compounds and Organic Spectroscopy, Science Press, Tsinghua, 1991, pp. 485–498.
[35] E. Gaudry, J. Aubard, H. Amouri, G. Lévi1, C. Cordier, Biopolymers 82 (2006) 399–404.
[36] H.T. Daryono, M. Shunsuke, A. Takehiro, Y. Naoki, I. Hidenari, J. Inorg. Biochem. 85 (2001) 219–228.
[37] S. Satyanaryana, J.C. Daborusak, J.B. Chaires, Biochemistry 32 (1993) 2573–2584.
[38] E.A. Máiíın, G.M. Barrett, M.H. Brian, J. Inorg. Biochem. 80 (2000) 257–260.
[39] Y. Ishikawa, A. Yamashita, T. Uno, Chem. Pharm. Bull. 49 (2001) 287–293.
[40] M.A. Sari, J.P. Battioni, D. Dupre, D. Mansuy, J.B. Lepecq, Biochemistry 29 (1990) 4205–4215.
[41] T. Jia, Z.X. Jiang, K. Wang, Z.Y. Li, Biophys. Chem. 119 (2006) 295–302.
[42] Y.Y. Fang, B.D. Ray, C.A. Caussen, K.B. Lipkowitz, E.C. Long, J. Am. Chem. Soc. 126 (2004) 5403–5412.
[43] M.J. Han, L.H. Gao, Y.Y. Lu, K.Z. Wang, J. Phys. Chem. B 110 (2006) 2364–2371.
[44] B. Armitage, C. Yu, C. Devadoss, G.B. Schuster, J. Am. Chem. Soc. 116 (1994) 9847–9859.
[45] D.T. Breslin, G.B. Schuster, J. Am. Chem. Soc. 118 (1996) 2311–2319.
[46] D. Rehm, A. Weller, Isr. J. Chem. 8 (1970) 259–263.
[47] S. Steenken, S.V. Jovanovic, J. Am. Chem. Soc. 119 (1997) 617–618.
[48] L.C. Xu, S. Shi, J. Li, S.Y. Liao, K.C. Zheng, L.N. Ji, Dalton Trans. 2 (2008) 291–301.
[49] N.V. Tkachenko, A.Y. Tauber, D. Grandell, P.H. Hynninen, H. Lemmetyinen, J. Phys. Chem. A 103 (1999) 3646–3656.
[50] P. Zhao, L.C. Xu, J.W. Huang, K.C. Zheng, B. Fu, J. Liu, H.C. Yu, L.N. Ji, Biophys. Chem. 135 (2008) 102–109.
[51] B. Armitage, Chem. Rev. 98 (1998) 1171–1200.
[52] D. Angelov, B. Beylot, A. Spassky, Biophys. J. 88 (2005) 2766–2778.